

APPLICATION OF OUT-OF-PLANE WARPING TO CONTROL ROTOR BLADE TWIST

Yannick Van Weddingen
Graduate Research Assistant
yannick.vanweddingen@gatech.edu
School of Aerospace Engineering
Georgia Institute of Technology
Atlanta, Georgia

Olivier Bauchau
Professor

olivier.bauchau@ae.gatech.edu

Sesi Kottapalli
sesi.b.kottapalli@nasa.gov
Flight Vehicle Research and Technology Division
NASA Ames Research Center
Moffett Field, California

Serkan Ozbay
Manager, Aerospace Programs
sozbay@aboutmtc.com

Yogesh Mehrotra
Vice President

ymehrotra@aboutmtc.com

Materials Technologies Corporation
Monroe, Connecticut

In rotorcraft flight dynamics, optimized warping camber/twist change is a potentially enabling technology to improve overall rotorcraft performance. Research efforts in recent years have led to the application of active materials for rotorcraft blade actuation, but their full scale performance often degrades significantly compared to bench top validation tests. An innovative concept is proposed wherein the typically closed section blade is cut open to create a torsionally compliant structure that acts as its own amplification device; deformation of the blade is dynamically controlled by three-dimensional out-of-plane warping. This 3D warping concept was evaluated analytically, numerically, and experimentally. Kinematics of the proposed system was validated, and general system design guidelines were determined. The response to aerodynamic pitching moments was investigated. As a result, a refined warping actuation concept, referred to as *full-blade warping*, is proposed. This innovative system has the potential for great design flexibility.

Introduction

Extensive research efforts have been devoted in recent years to the application of active material actuation for rotorcraft blades. The use of piezoelectric actuators to deflect the trailing edge surface, the leading edge, or the tip section of rotor blades has been widely investigated (Refs. 1-6) Piezoelectric materials are the preferred candidates for high-frequency on-blade actuation due to the ease of control provided by their rapid response to the applied electric field. In such applications, piezoelectric actuators would be

typically expected to induce a significant change in the shape of the blade, with the aim of inducing large changes in airloads. However, current piezoelectric materials are inherently constrained by limited authority because of their very small linear actuation strain/displacement capability. Therefore, an amplification of the actuator output is required to achieve a larger strain, and hence, the desired dynamic airfoil twist/camber deformation. Mechanical amplification devices have been used to amplify the available piezoelectric actuation (Refs. 7-10) While this approach has met with some success, the performance of such actuation methods in a demanding, long-term, fielded, full-scale rotor blade environment is deemed inadequate. Their performance may be degraded by friction, free play, and aerodynamic and inertial loads. The additional complexity of the required amplification mechanisms goes against the reason for using active material actuation, i.e., the development of a simple reliable actuation scheme with no moving components.

Presented at the American Helicopter Society Aeromechanics Specialists' Conference, San Francisco, California, January 20-22, 2010. Copyright © 2010 by the American Helicopter Society International, Inc. All rights reserved.

Finally, many full-scale configurations tested thus far are limited to actuating a discrete trailing or leading edge deflection system with limited authority, and thus are subject to the aerodynamic inefficiencies of a limited span application.

In an alternative approach, the strain induced by embedded actuators was used to cause overall twisting of the complete rotor blade (Refs. 11-17). Here again, success was limited in terms of the magnitude of the resulting blade deformation. While more efficient than the first approach described above, the embedded actuator approach has the inherent limitation that relatively weak actuators are used in an attempt to deform a nominally stiff structure. Additionally, this approach requires that the actuators be structurally integrated into the blade spar thus making the in-service repair of any failed actuators very difficult.

In contrast to the current approaches, this paper presents a novel three-dimensional concept, in which the blade section is cut open to create a torsionally compliant structure that acts as its own amplification device, and in which out-of-plane warping controls the blade deformation. This innovative concept provides a means for dynamically changing the camber/twist of a rotor blade, without requiring the actuator to deliver excessively high forces. Moreover, our 3D warping concept could be applied to trailing edge flaps, the aft section of a rotor blade behind the D-spar, or even to the full chord length of the blade.

In this paper, first a general description of the 3D warping concept is presented, highlighting the design flexibility provided by the 3D concept. Second, the theoretical background behind this concept is summarized, including the necessary modifications to the classical Vlasov beam theory to ensure the applicability of its results. Then, some experimental results obtained on a portion of an actual UH-60 helicopter blade are presented. Finally, details of the performed static and dynamic finite element analyses are discussed, leading to the final proposed 3D warping concept based on the design guidelines that were identified throughout the current research program.

Out-of-plane warping for twist control

In a radical departure from the current approaches for camber control, a unique concept is proposed in which the typically closed blade section is cut open to create a torsionally compliant structure that acts as its own amplification device. The integration of a moderate twist rate created through 3D warping along the length of the blade translates into a sizeable tip twist in the case of these typically slender beam structures. The deformation of the blade is controlled by out-of-plane warping resulting in three-dimensional morphing of the blade.

To illustrate this innovative concept, Fig. 1 depicts a rotor blade with a trailing edge flap; for simplicity, the support structure of the flap is not shown. The trailing edge flap is a torsionally compliant structure with an open section susceptible to out-of-plane cross-sectional warping. Actuation of the out-of-plane warping by inducing a relative axial displacement between the two sides of the cut then leads to significant twisting of this component; this is exactly the reciprocal effect of the well-known out-of-plane warping induced by twisting (Ref. 18). The “F” symbol in the figure shows the point at which actuation is applied. In view of the very low torsional stiffness of open sections, little actuation effort is required to warp the section, resulting in significant twisting.

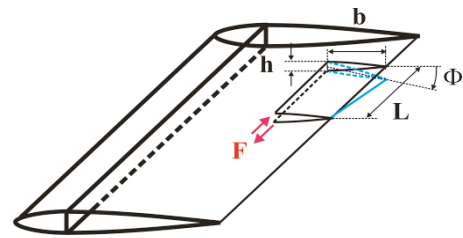


Fig. 1. Warping actuation concept applied to a rotorcraft elevon.

As shown in Fig. 1, this concept can be applied to a 15% length of the chord trailing edge flap by actuating only a small portion of the airfoil. In the same manner, it is also possible to actuate a 75% of chord flap extending over the entire length of the blade to create a large camber change for the whole rotor blade. This concept is illustrated in Fig. 2. The resulting camber change over the entire blade could be used to provide cyclic control, thereby eliminating the need for swashplates altogether. Additionally, the larger span extent reduces the aerodynamic losses related to end effects on a limited span flap.

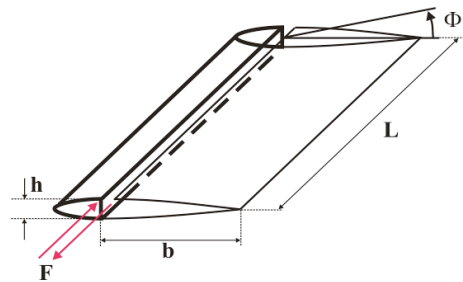


Fig. 2. Warping actuation concept applied to 75% flap design.

For the illustrated concept to work, a double joint design is needed, as illustrated in Fig. 3. This joint allows the aft portion of the blade to rotate as a rigid body, an essential feature for the eventual success of the 3D warping concept. Additionally, the joint design would also allow for the axial

warping actuation needed to control the blade's shape. Figure 4 gives a possible design for this double joint. It also presents the option for a redesign of the blade's structural composition itself. The typical honeycomb core used in rotor blades may not be entirely necessary; similar stiffening effects could be achieved through a sandwich wall construction as suggested in the figure. The 75% of chord flap configuration with double joint was extensively studied, and related results showing the benefits and drawbacks are included in the following sections.

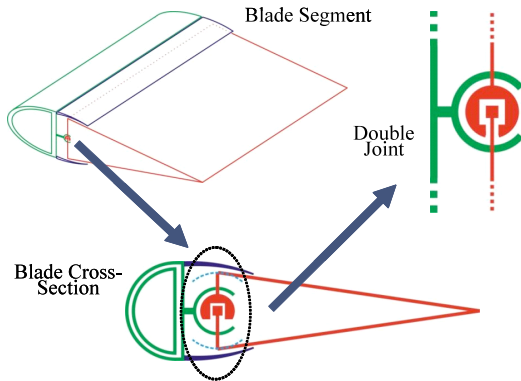


Fig. 3. Double joint providing rigid rotation of the aft part.

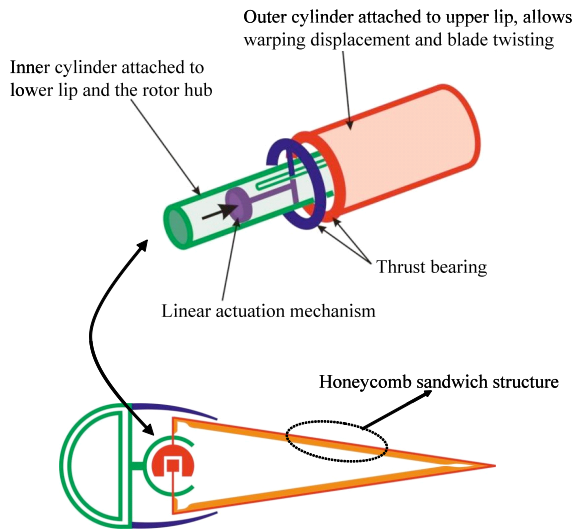


Fig. 4. Double joint design and stiffened aft section walls.

Depending on the points of application of the actuators, two main configurations can be realized: distributed actuation or concentrated actuation. Figure 5 illustrates the difference between these two actuation concepts. Concentrated actuation, Fig 5(a), would be achieved using a single, relatively large actuator placed close to the rotor hub. It

would possibly be an electromechanical or lead-screw system. Distributed actuation, Fig 5(b), would be obtained by placing several relatively small actuators along the blade span. The actuators can be electromechanical or possibly even based on piezostacks, given the very low actuation stroke amplitude requirement.

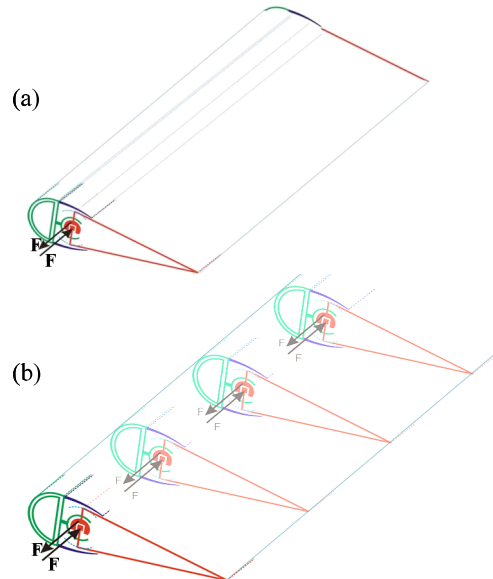


Fig. 5. (a) Concentrated actuation vs. (b) distributed actuation.

Theoretical background

Classical Vlasov beam theory

Consider a thin-walled beam in torsion, as shown in Fig. 6.

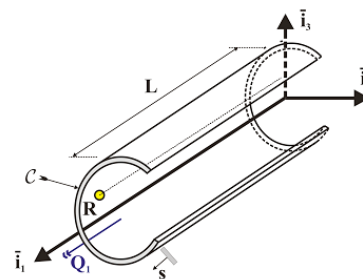


Fig. 6. A thin-walled beam subject to torsion.

The axis of the beam is along \bar{i}_1 , while \bar{i}_2 and \bar{i}_3 define the plane of the cross-section. C denotes the contour line defining the cross-sectional geometry, and s the associated curvilinear coordinate. Point R , of cross-sectional coordinates x_{2r} and x_{3r} , corresponds to the as of yet unknown center of rotation about which the beam twists.

First, assume the following displacement field

$$\begin{aligned} u_1(x_1, s) &= \Psi(s) \kappa_1(x_1) \\ u_2(x_1, s) &= -(x_3 - x_{3r}) \phi_1(x_1) \\ u_3(x_1, s) &= (x_2 - x_{2r}) \phi_1(x_1) \end{aligned} \quad (1)$$

The axial displacement field u_1 is proportional to the twist rate $\kappa_1 = \frac{d\phi_1}{dx_1}$ and is characterized by an unknown cross-sectional warping function $\Psi(s)$. The displacement components u_2 and u_3 describe the rotation of the cross-section by a twist angle ϕ_1 . Using the strain-displacement relationships and the constitutive equations, and allowing for non-uniform torsion, $\frac{d\kappa_1}{dx_1} \neq 0$, the only non-vanishing stress components are

$$\sigma_1 = E\varepsilon_1 = E\Psi(s) \frac{d\kappa_1}{dx_1} \quad (2)$$

$$\tau_{12} = G\gamma_{12} = G \left[\frac{d\Psi}{dx_2} - (x_3 - x_{3r}) \right] \kappa_1 \quad (3)$$

$$\tau_{13} = G\gamma_{13} = G \left[\frac{d\Psi}{dx_3} + (x_2 - x_{2r}) \right] \kappa_1 \quad (4)$$

In a thin-walled open-section beam, the tangential shear stress varies linearly through the thickness and vanishes along the contour center line. Hence, using Eqs. (3) and (4) and projecting onto the tangential direction, the tangential shear stress takes the form

$$\tau_s = G \left(\frac{d\Psi}{ds} + r_r \right) \kappa_1 = 0 \quad (5)$$

where r_r is the distance from the twist center to the tangent to the contour. Hence, the unknown warping function must satisfy

$$\frac{d\Psi}{ds} = -r_r = - \left(r_o - x_{2r} \frac{dx_3}{ds} + x_{3r} \frac{dx_2}{ds} \right) \quad (6)$$

where r_o is now the distance from the origin of the axes to the tangent to the contour. Introducing a function $\Gamma(s)$ such that

$$\frac{d\Gamma}{ds} = -r_o \quad (7)$$

the warping function can be obtained as

$$\Psi(s) = \Gamma(s) + x_{2r} x_3 - x_{3r} x_2 + a \quad (8)$$

in which a is an integration constant which can be determined through the vanishing of the axial force resultant

$$0 = N_1 = \int_C \sigma_1 t ds \quad (9)$$

Using Eqs. (2), (8) and (9), the integration constant can then be found as

$$a = -\frac{1}{S} \int_C E\Gamma t ds \quad (10)$$

In the classical Vlasov theory, the center of twist can be shown to be at the shear center (Ref. 18.) The warping function $\Psi(s)$ is fully determined, and can be used to identify all the displacement, strain and stress components using Eqs. (1), (2), (3) and (4). Detailed derivations may be found in Ref. 18.

Energy approach to non-uniform torsion

Once the warping function is determined for the beam cross-section, the energy approach can be used to investigate the behavior of the structure under different applied loads and boundary conditions. In this approach, we assume a displacement field of the form

$$\begin{aligned} u_1(x_1, s) &= \Psi(s) \alpha(x_1) \\ u_2(x_1, s) &= -(x_3 - x_{3k}) \phi_1(x_1) \\ u_3(x_1, s) &= (x_2 - x_{2k}) \phi_1(x_1) \end{aligned} \quad (11)$$

where the axial displacement is assumed to be proportional to an unknown function $\alpha(x_1)$ through the warping function $\Psi(s)$. For the open thin-walled beam, considering Eq. (11), the non-zero strain field components can be written

$$\varepsilon_1 = \Psi(s) \frac{d\alpha}{dx_1}, \quad \gamma_s = \left(\frac{d\phi_1}{dx_1} - \alpha \right) r_k, \quad (12)$$

The strain energy of the beam is then

$$A = \frac{1}{2} \int_0^L \left[H_{11w} \left(\frac{d\alpha}{dx_1} \right)^2 + I_p \left(\frac{d\phi_1}{dx_1} - \alpha \right)^2 + H_{11} \left(\frac{d\phi_1}{dx_1} \right)^2 \right] dx_1 \quad (13)$$

where H_{11w} , H_{11} and I_p represent the torsional stiffness due to warping, the classical torsional stiffness, and the torsional stiffness coefficient due to non-uniform through-the-thickness variation of shear stress; these are defined as

$$\begin{aligned} H_{11w} &= \int_C E\Psi^2 t ds \\ I_p &= \int_C Gr_k^2 t ds \\ H_{11} &= G\frac{I^3}{3} \end{aligned} \quad (14)$$

The principle of minimum potential energy can then be invoked based on the total potential:

$$\Pi = A - (\text{Energy due to externally applied loads}) \quad (15)$$

This formulation leads to a set of differential equations that need to be solved based on a set of applied loads and boundary conditions.

Open triangular section

In this study, we considered a thin-walled beam with open triangular section representing the aft section of a rotor blade. This section depicted in Fig. 7 could be used to model both concepts described in the previous section, depending on how the left-hand-side is constrained. The section's geometry is detailed in Fig. 8.

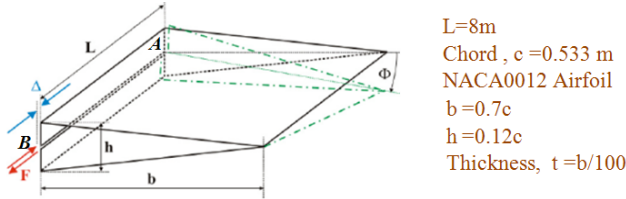


Fig. 7. Model for the aft part of the blade.

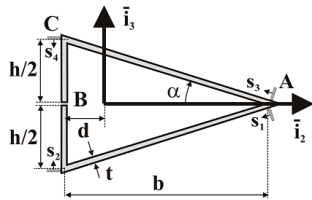


Fig. 8. Open triangular section geometry.

Based on the previously presented formulation, the warping function for the cross-section was determined to be

$$\begin{aligned} \Psi_1 &= -\frac{\sin \alpha}{1 + \sin \alpha} \frac{bh}{4} \bar{s}_1; \\ \Psi_2 &= \frac{(2 + 3 \sin \alpha) \bar{s}_2 - \sin \alpha}{1 + \sin \alpha} \frac{bh}{4}; \\ \Psi_3 &= -\Psi_1; \quad \Psi_4 = -\Psi_2 \end{aligned} \quad (16)$$

A representation of this warping function is depicted in Fig. 9.

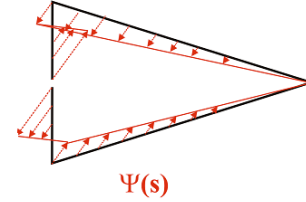


Fig. 9. Warping function for open triangular section.

Then, in the framework of the classical warping model, the cross-sectional parameters related to the warping behavior are:

$$H_{11} = \frac{2}{3} Gt^3 l (1 + \sin(\alpha)) \quad (17)$$

$$H_{11w} = \frac{1}{48} \frac{4 + 3 \sin(\alpha)}{1 + \sin(\alpha)} Etb^2 h^3 \quad (18)$$

$$I_p = \frac{1}{4} \frac{\sin(\alpha)^2 + 8 \sin(\alpha) + 4}{1 + \sin(\alpha)} Gthb^2 \quad (19)$$

As a representative case, consider the case of concentrated actuation provided at point B. In this configuration, the tip section rotation and applied load were determined in terms of the relative displacement Δ as

$$\begin{aligned} \phi_L &= \left(\frac{\Delta}{b}\right) \left(\frac{L}{h}\right) \frac{I_p}{I_p + H_{11}} \frac{\sinh(k)}{\cosh(k)} \frac{1}{k} \\ F &= \left(\frac{\Delta}{b}\right) \left(\frac{L}{h}\right) \frac{I_p}{I_p + H_{11}} \frac{H_{11}}{bh} \frac{\sinh(k)}{\cosh(k)} \frac{1}{k} \\ k^2 &= \frac{I_p H_{11} L^2}{H_{11w} (I_p + H_{11})} \end{aligned} \quad (20)$$

It can be seen that these quantities are strongly dependent on the parameter k which itself is a function of the sectional stiffnesses. Similar resulting equations can be obtained for different loading configurations, such as the prescribed displacement or distributed load cases, which both result in the same analytical solution

$$\phi_L = \left(\frac{\Delta}{b}\right)\left(\frac{L}{h}\right)\frac{I_p}{I_p + H_{11}}$$

$$fL = \left(\frac{\Delta}{b}\right)\left(\frac{L}{h}\right)\frac{I_p}{I_p + H_{11}}\frac{H_{11}}{bh} \quad (21)$$

Modified Vlasov theory

The classical Vlasov beam theory for torsion and warping needed to be modified for the purposes of this study. Indeed, this theory assumes no constraints outside of the beam boundary conditions, and as a consequence places the center of twist at the location of the shear center. However, in our applications, the base of the triangular section will be constrained in various ways depending on its connection with the D-spar. This effectively constrains the center of twist to a particular point in the cross-sectional plane, point B in Fig. 8. This will modify the final expression of the warping function as computed by Eq. (8), and therefore will also change the sectional coefficients related to torsion and warping. In the specific case of the open triangular section, one now finds

$$H_{11w} = \frac{1}{6}(1 + 3\sin(\alpha))Et b^2 h^2 l \quad (22)$$

$$I_p = Gthb^2 \sin(\alpha) \quad (23)$$

$$k^2 = \frac{H_{11}L^2}{H_{11w}} \frac{1}{1 + H_{11}/I_p} = \frac{L^2}{H_{11w}} \frac{1}{\frac{1}{H_{11}} + \frac{1}{I_p}} \quad (24)$$

The solutions of the differential equations are still valid, but their expressions need to be updated with these new coefficient values. It will be shown in later sections that when the aft part of the blade is correctly constrained, these new equations correlate well with finite element results, while using the usual coefficients does not capture the behavior of the blade.

Preliminary experimental results

A bench-top test was conducted using a 2.5-foot-long section of an actual UH-60A rotorcraft blade provided by Sikorsky Aircraft. This test piece was cut open along the blade span in the aft section as illustrated in Fig. 2. It was secured on a bench top where spanwise forces, provided through a lead-screw mechanism, were applied along the cut-open section as shown in Fig. 10 below. The section was stiffened along the cut edge and support guides were used to simulate a typical slider joint that would be used in a rotor blade to connect the aft section to the D-spar of the blade. The applied axial force, the resulting twist as well as the out-of-plane warping displacement along the cut edge were measured. Three sets of tests were performed: warping actuation without the support guides, warping actuation with

support guides, and warping actuation with support guides after the honeycomb core was removed.

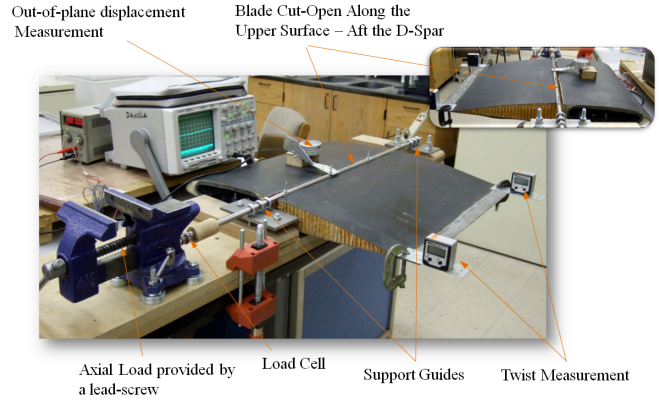


Fig. 10. Experimental set-up.

First, the support guides were removed, essentially creating a free boundary condition along the upper lip of the blade section. The honeycomb core was left intact except at the location of the cut. Figure 11 shows that in this configuration, an actuation load of about 400 lb generated a twist of about 0.6 degrees at the tip section of this 2.5 ft blade.

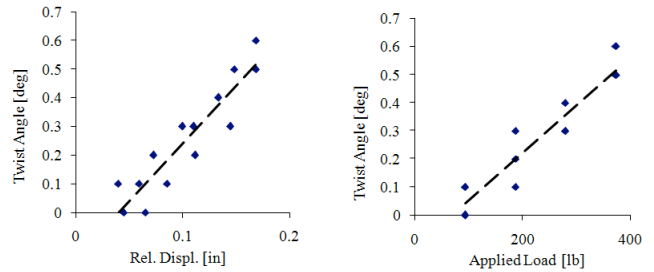


Fig. 11. Blade section without support guides: twist angle vs. relative displacement and applied load.

A detailed look at the deformed section of Fig. 12 reveals that the structure twists through shell bending along the lower surface of the blade.



Fig. 12. Blade section without support guides: detail of the deformation through shell bending modes.

Next, the above test was repeated in the presence of the support guides; they simulate a sliding joint attaching the upper edge of the cut aft section to the D-spar. Figure 13 shows that a larger actuation load is required to generate a tip twist of similar magnitude as the first case.

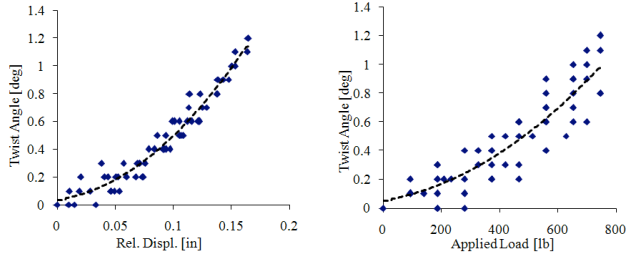


Fig. 13. Blade section with support guides: twist angle vs. relative displacement and applied load.

An inspection of the deformed section again reveals that the section twisting occurs through shell bending, as can be seen in Fig. 14.

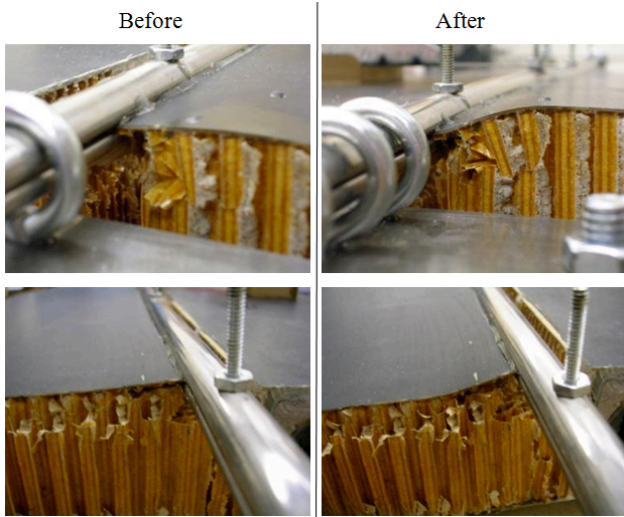


Fig. 14. Blade section with support guides: detail of the deformation exhibiting shell bending modes.

Finally, the honeycomb core was removed from the blade structure, essentially creating a thin-walled aft section. As expected, this generated a noticeably more compliant structure compared to the original blade configurations from the previous cases. Results of the tests performed in the presence of support guides are shown in Fig. 15. It can be seen that when the honeycomb core was removed, the section required far less actuation load compared to the foregoing two cases.

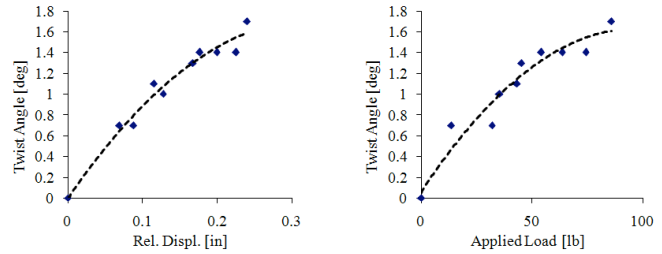


Fig. 15. Blade section without honeycomb core and with support guides: twist angle vs. relative displacement and applied load.

However, the deformations in this case were obtained through more severe shell bending modes, Fig. 16, as rigid rotation of the aft section is prevented.



Fig. 16. Blade section without honeycomb core and with support guides: extensive shell deformation is apparent.

These experiments are in full agreement with the reasoning behind the introduction of double joint, Fig. 3, that rigid rotation of the aft section is desired in order to take full advantage of the blade warping concept. Also, one can conclude that a design including a full honeycomb core filling the aft section may be detrimental to this morphing concept, as it stiffens the aft portion of the blade. An optimized design would be needed, to allow for a large enough range of warping motion, while still maintaining the structural integrity of the blade in flight.

Static analyses

Comparisons with the theory

To verify the validity of the analytical formulations, a finite element shell model of the section illustrated in Fig. 7 was created using ABAQUS. Figure 17 shows a representative model. The FE analysis used 3D shell elements, with different boundary conditions along the edges where the section is cut open, depending on the desired actuation mechanism. In the following discussions, the rectangular coordinate system associated with this FE model has its axes labeled 1, 2 and 3, where 1 designates the axial direction, normal to the plane of the blade cross-section.

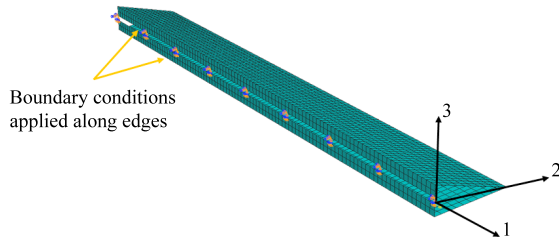


Fig. 17. ABAQUS shell model for 75% flap configuration.

As stated earlier, in a typical rotor blade application, the flap section has to be attached to the D-spar of the rotor blade through a sliding joint allowing out-of-plane warping to occur freely. This is achieved by co-locating the actuation and the axis of rotation by a double joint type connection. On one hand, it allows for relative sliding between the lower and the upper lip of the cut for out-of-plane warping; and on the other hand, it allows rotation of the aft blade section as a rigid body about this axis. In this case, however, it is necessary to use the modified Vlasov theory, forcing the axis of rotation of the section at the correct location, rather than at the shear center. This adaptation affects the values of the warping function and the sectional quantities related to warping.

The boundary conditions were defined in ABAQUS to reflect this modified configuration. The in-plane motions were constrained while free rotation about the slider joint axis was maintained for the upper and lower lips. Figures 18 and 19 show the numerical results obtained with this set of boundary conditions (“ABAQUS”), as well as analytical results obtained for both this set of boundary conditions (“analytical-slider”) as well as the set of free boundary conditions used in the classical approach to warping (“analytical-free”). The results of the analysis for concentrated actuation in Fig. 18 show that the predictions of the analytical formulation with the correct sectional constants correlate well with the ABAQUS shell model predictions for the kinematic relationship. However, the force-displacement relationships do not correlate as well due to the inclusion of nonlinear effects in the numerical runs. In addition, it is clear that the classical theory does not predict the correct results. Similar observations can be made for the distributed actuation case shown in Fig. 19. Note that the two analytical solutions are very close, as can be seen from Eqs. (21), where $I_p / (I_p + H_{11}) \approx 1$ in both cases. Based on these analyses, we conclude that the Vlasov beam theory properly models the kinematics of the 3D warping concept provided that the assumptions made are correct.

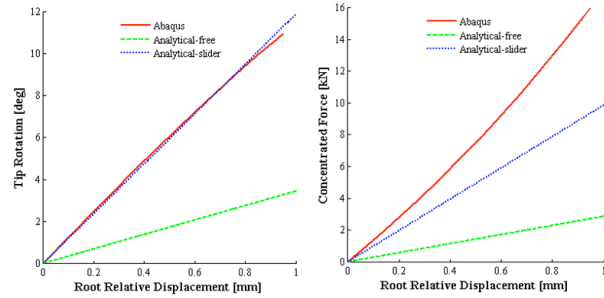


Fig. 18. Comparison of numerical and analytical results for concentrated actuation with double joint connection: tip twist and concentrated force vs. relative warping displacement at the root.

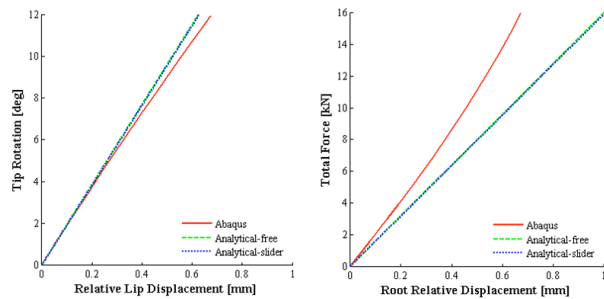


Fig. 19. Comparison of numerical and analytical results for distributed actuation with double joint connection: tip twist and total warping force vs. relative warping displacement at the root.

Distributed vs. concentrated actuation

The actuation of the system can be achieved in two distinct ways: distributed actuation along the edge, or concentrated actuation where a single point load is applied at one end of the structure. In this section, we will investigate the effects of these two options using static ABAQUS analyses. Figure 20 shows the model with a 200 N/m² applied surface load.

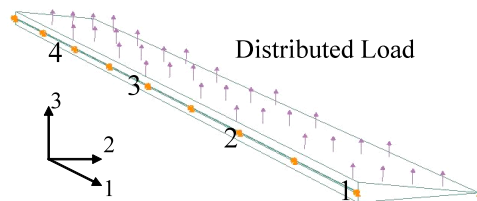


Fig. 20. Static ABAQUS model with various possible locations (denoted by 1-4) for actuator placement.

This surface load was reacted by a number of actuators located along the span of the blade, as described in Table 1. Cases 1, 2 and 3 represent several levels of point load actuation, with increasing numbers of actuators. Case 1

corresponds to the pure concentrated actuation scenario. On the other hand, case 4 in the table represents an idealized distributed actuation case where the load is assumed to be applied continuously along the open lips.

Table 1. Various combinations of actuator locations.

Case	Actuator Locations
1	1
2	1, 3
3	1, 2, 3, 4
4	Idealized distributed actuation

The results of this analysis are shown in Fig. 21. The total reaction represents the actuation load required to keep the zero stroke condition at the load application points due to the applied external load. It can be seen that the concentrated actuation case is very compliant compared to the distributed actuation case and cannot react the applied external load efficiently. The structure rotates by about 25 degrees at the blade tip in the concentrated actuation case, whereas in the distributed actuation case, the structure barely rotates at the blade tip. However, it should be noted that, with only a few concentrated point actuators scattered along the blade span, it is still possible to mimic a distributed actuation scenario quite effectively. The results show that distributed actuation (case 4) would have a better control authority for the success of the 3D warping concept, but close to ideal actuation performance can also be achieved when multiple point load actuators are distributed along the blade span (case 3).

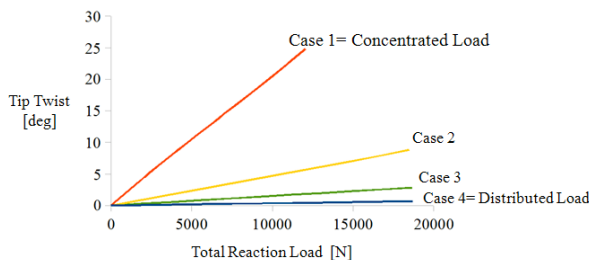


Fig. 21. Reaction to the external load based on different actuation cases.

Axial reinforcement

The results of the above analysis raise questions regarding the ability of the concentrated actuation system to carry its reaction capability across the blade span. One means of improving its performance in this respect would be to stiffen the line of action of the applied load along the blade span, such that its effects can be felt farther from the point of

application. Figure 22 illustrates the stiffening of the section at location “K”.

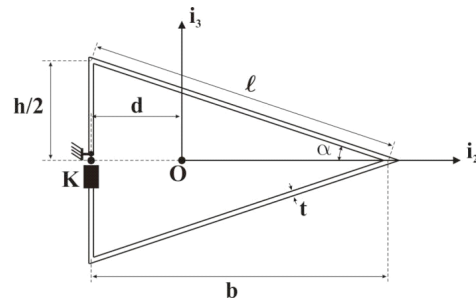


Fig. 22. Stiffened line of action at K.

This section was analyzed in ABAQUS with different stiffness values assigned to the support region, while the rest of the cross-section is assumed to be aluminum. The results of this analysis are shown in Fig. 23. As the stiffness value of the support increases, the distributed and concentrated actuation cases show increasingly similar responses. Therefore, it is reasonable to extend the argument that a number of actuators along the blade span with a stiffened line of action could generate the required actuation effectiveness for the 3D warping concept.

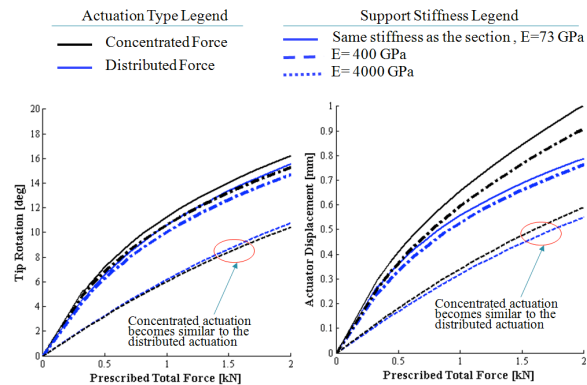


Fig. 23. Concentrated vs. distributed actuation for different values of the support stiffness.

Dynamic analysis

Dynamic loads vs. static loads

In dynamic environments, inertial forces are typically higher than their static counterparts and have been reported to become a barrier to the success of many active actuation concepts. To investigate the inertial effects, ABAQUS dynamic analysis procedures were used to study the behavior of the double-jointed 75% flap configuration. In the model used for this analysis, several linear dashpots were

placed along the span of the blade to simulate some form of aerodynamic damping on the structure. The out-of-plane warping was controlled by applying a prescribed sinusoidal relative displacement between the open lips.

In dynamic actuation cases, inertial forces increase the load requirement compared to the static case, unless the excitation and the system's natural frequencies coincide. Figure 24 illustrates the effect of excitation at the resonant frequency. For $\omega_{excitation} / \omega_{natural} = 1$, the dynamic load requirement is minimum and is less than the static load requirement.

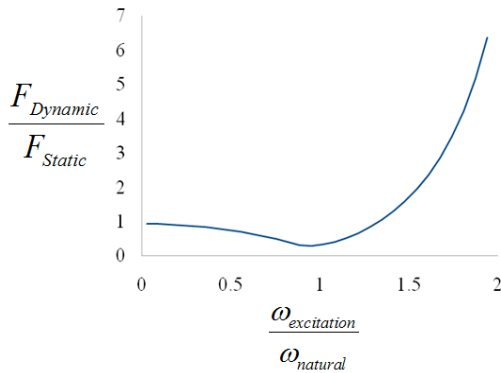


Fig. 24. Effect of resonant design on actuator load requirement.

In applying the 3D warping concept to swashplateless rotors, the interest lies with excitations of the system at 1/rev. But typically, rotor blades are tailored to restrict the first torsional frequency to be above 4/rev rotor frequency. However, since this novel concept essentially creates an open section with respect to the actuator load, it would be possible to tailor the flap configuration's first torsional frequency to be close to 1/rev to take advantage of the resonant design. To investigate this possibility, a configuration with a composite sandwich wall design was used. Table 2 details the layout used for the sandwich wall all around the triangular cross-section.

Table 2. Composite sandwich wall lay-up.

Material	Thickness (mm)	Ply angle (deg)
Carbon-Epoxy	1	0
Carbon-Epoxy	1	90
Balsa	12	0
Carbon-Epoxy	1	90
Carbon-Epoxy	1	0

A linear perturbation analysis in ABAQUS identified the system's first torsional frequency as 3.877 Hz. Then, the system was excited at 4.3 Hz, the 1/rev frequency for a typical UH-60 rotor, using a prescribed relative displacement time history $\Delta(t) = 1.5 \sin(2 \cdot \pi \cdot 4.3 \cdot t)$ mm. Figure 25 shows the time history of the required actuation load to sustain the prescribed sinusoidal relative displacement. It is seen that the system requires considerably lower steady state actuation loads compared to the static case. Hence, careful design of the warping-enabled section to take advantage of resonances would lead to more efficient systems.

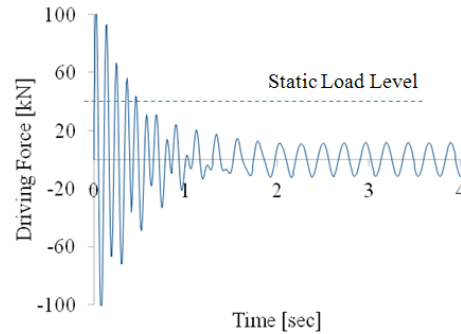


Fig. 25. Dynamic response to excitation at 4.3 Hz.

Effects of external loads

The response of the warping actuated blade to the applied aerodynamic loads was also investigated. Theodorsen's theory for an airfoil with a flap (Ref. 19) was used in order to determine the aerodynamic load levels to be reacted by the system. Figure 26 graphically shows a comparison between the conventional case where the whole section rotates about the quarter chord location according to collective and cyclic inputs, and the case at hand where the rotation is limited to the 75% aft portion of the blade section.

Figure 27 shows the evolution of the required cyclic flap angle as the flap length changes, such that the total lift generated is identical to that of a rigid blade with a cyclic pitch angle as indicated on the figure. It can be seen that, above 60% flap length, the required cyclic pitch angles are almost the same. This result points to the fact that the 3D warping concept with 75% flap is a viable option for designing a swashplateless rotor in terms of the generated lift. Small flaps (<20% chord) would, however, require very large pitch angles to achieve the same result.

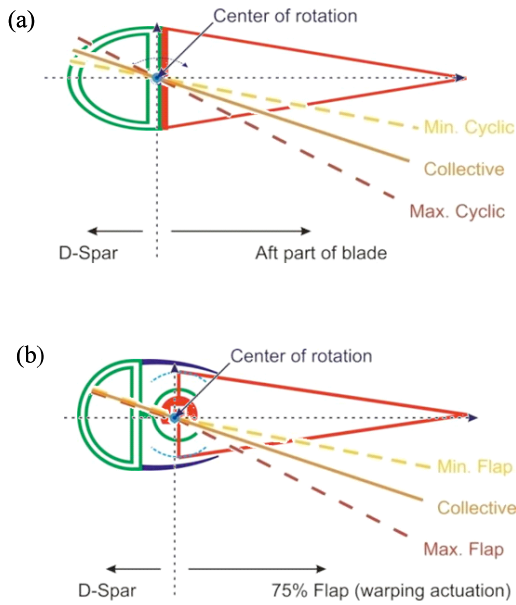


Fig. 26. (a) Typical rotor blade vs. (b) 75% flap configuration.

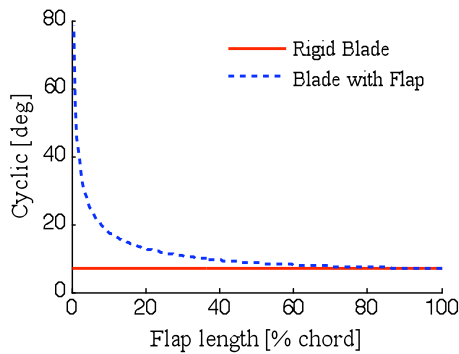


Fig. 27. Cyclic angle comparison for equal sectional lifts.

Following these observations, Theodorsen's theory was used to calculate the blade loads to be used as inputs to the structural analysis of the system. The total blade loads, as measured at the blade root, are shown in Fig. 28 for a typical baseline rigid blade and a blade with 75% flap. Notice that the total lifts were made to match in both cases. It can be seen that the flap pitch moments about the flap hinge are much higher than the total airfoil pitch moments about the quarter chord. The flap hinge moment is about 2000 Nm, whereas the total quarter chord moment is around 400 Nm for the flapped blade and 50 Nm for the rigid blade. Unfortunately, the 75% flap design must react the large 2000 Nm aerodynamic moment.

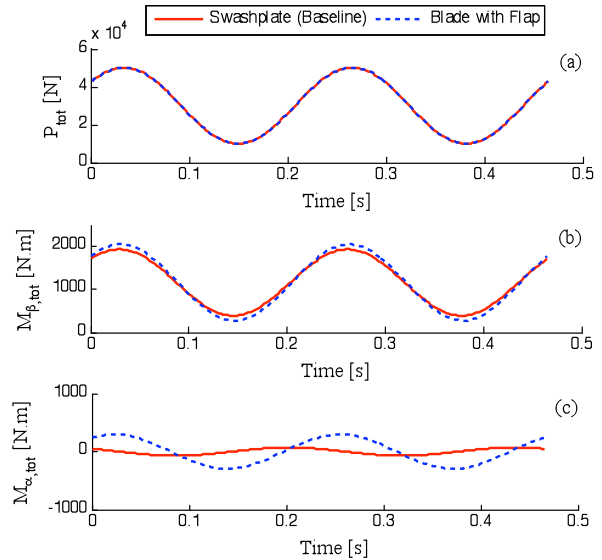


Fig. 28. Total lift, total flap moment about flap hinge, and total pitching moment about the quarter chord.

To confirm the issues posed by such large forces, an ABAQUS model was used to statically evaluate the response of the 75% flap to the aerodynamic flap moment about the hinge. A distributed pressure load was applied to simulate the aerodynamic pressure on the structure, leading to a total root moment of about 2000 Nm. It was found that the system requires an elevated actuator load of more than 400 kN to react this moment. Next, a two-step analysis procedure was performed, in which the structure was first twisted by warping actuation resulting in about 30 degrees of blade tip twist, and afterwards was loaded with the same external pitching moment (2000 Nm). Figure 29 shows that the system requires very large actuator loads above 500 kN to react the external loads. Moreover, the twist achieved by warping actuation was drastically reduced, due to the opposite elastic twist of the blade under the aerodynamic moments.

These results point to the leverage effect generated by the 3D warping actuation concept with 75% flap. The essence of this concept resides in the fact that small warping displacements create large tip twists, thus creating the desired amplification; however, it also results in the fact that small applied tip torques will require large equilibrating action forces as well.

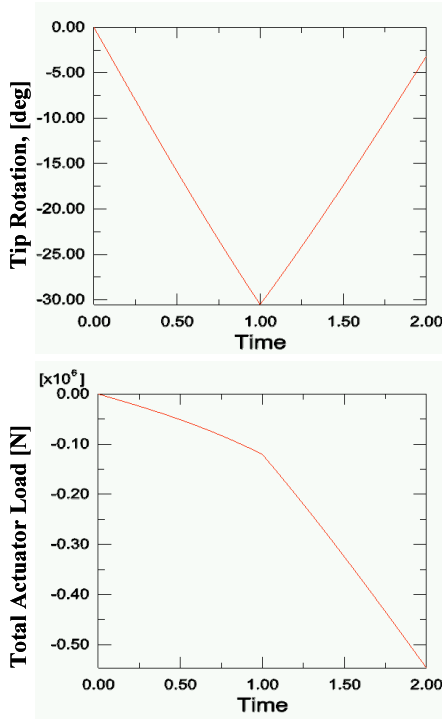


Fig. 29. Response of 75% flap configuration to external pitching moments.

Full blade warping control

Finite element analysis results

The concept presented above, while promising in certain aspects, also showed the shortcomings of the 75% flap design of the warping actuated blade. Figure 30 illustrates a typical lift distribution over an airfoil. It can be seen that the way the double-jointed concept is constructed, the warping actuated flap has to react the moment generated by the lift over the aft section of the rotor blade. However, when the airfoil is considered as a whole, the total moment about the quarter chord is minimal due to force equilibrium.

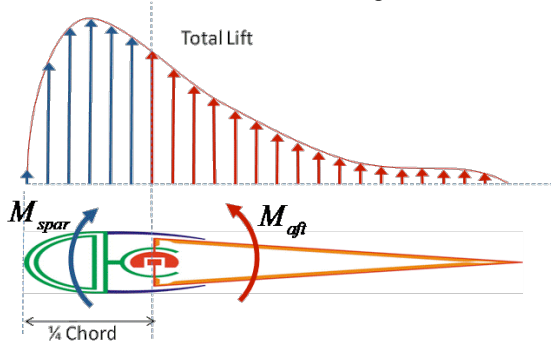


Fig. 30. Pressure distribution over a typical airfoil.

This observation leads to the most recent innovative concept of **full-blade warping**, where the blade is cut open along the entire length of both the leading and the trailing edges, thus forming a torsionally compliant structure. This unique structure takes the shape of an I-beam with curved upper and lower flanges, and with the airfoil vertical web forming the I-beam's vertical web, as shown schematically in Fig. 31. When actuated along the leading edge, the entire airfoil rotates as a rigid body around the pitch axis, resulting in large relative tip twists. Ideally, the D-spar is located close to the quarter chord location to take advantage of the low total aerodynamic moments.

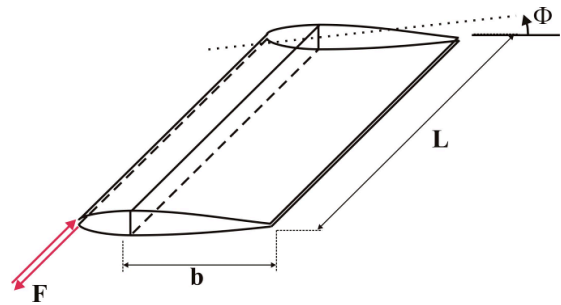


Fig. 31. Full-blade warping concept.

An ABAQUS model of this new concept was constructed using 3D shell elements and is shown in its deformed configuration in Fig. 32. A static prescribed displacement analysis was performed to demonstrate the twisting of the new blade configuration. The results are shown in Fig. 32 as well. The concept allows the blade to achieve a 30 degree tip twist for as little as 2 mm of relative displacement applied along the leading edge open lips. This analysis verifies that warping actuation is not inherent to any particular shape of the airfoil and is effective for open sections of any shape, thus providing unique and great design flexibility.

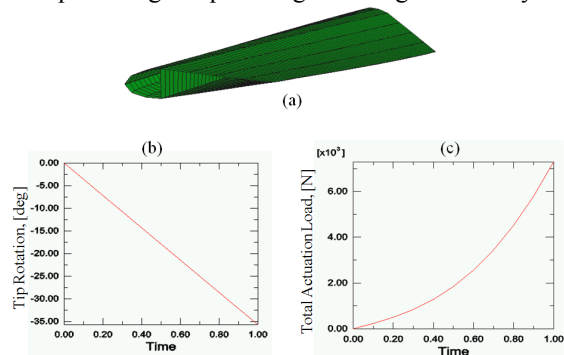


Fig. 32. Response to prescribed displacement: (a) deformed configuration, (b) tip rotation, and (c) total actuation load.

The response of the full-blade warping concept to external loads was investigated next, as before. It was found that the 50 Nm aerodynamic pitching moment about the quarter chord would require only about 20 kN of actuator load, resulting in less than 0.5 degrees of tip twist. By comparison, the 75% flap design required over 400 kN of actuation load to react a total moment of about 2000 Nm.

Practical implementation

This proposed full-blade warping concept is radically different from the current state-of-the-art in rotor blade sectional configurations, and its aeroelastic implications are yet to be explored. However, in addition to sensibly lower aerodynamic moments compared to the 75% flap configuration, several possible mechanical and aerodynamic benefits can be predicted for this innovative design. With actuation at the leading edge cut, the actuators would be placed forward of the quarter chord point, which is an inertially preferred location for additional weight. Moreover, the typical overall airfoil shape, with relatively well-defined aerodynamic forces, would be maintained.

A schematic of a possible practical configuration is illustrated in Fig. 33. The open leading and trailing edges would be hermetically sealed using relatively soft elastomeric seals, thus fully protecting the inside of the rotor blade against adverse effects such as sand erosion, while allowing the required relatively small out-of-plane warping displacement to take place along the cut edges. Other design considerations would include the erosion cap at the leading edge, as well as the preferred placement of the hermetically sealed actuator.

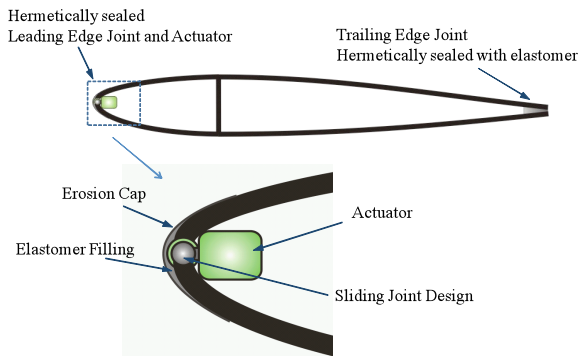


Fig. 33. Application of full-blade warping concept.

Conclusions

The key observations, based on substantiating analyses and limited bench-top testing, are as follows:

i) Vlasov beam theory has been shown to properly model the kinematics of the warping concept. Results have been

validated through the use of the 3D shell models from the commercially available analysis software ABAQUS.

ii) The general design guidelines regarding a viable flap concept have been determined, as follows:

- a) Only 1 to 2 mm relative displacement is required
- b) The blade sections should rotate rigidly about a point

iii) The response of the original 75% flap configuration to external aerodynamic pitching moments has been computed. It was determined that such a flap configuration would be excessively compliant to external loads, and the associated actuator load requirements would be excessively high.

iv) Subsequent to Item iii) above, the *Full-Blade Warping* concept has been proposed and analyzed. This concept takes advantage of the low aerodynamic moments about the quarter chord.

v) In general, the warping actuation is not inherent to a particular shape of the airfoil, such as a trailing edge flap or a 75% flap.

vi) The warping actuation is effective for open sections of any shape, providing unique and great design flexibility.

Acknowledgments

This Phase I SBIR study is funded by the NASA Subsonic Rotary Wing Project.

References

1. Bernhard, A., and Chopra, I., "Trailing Edge Flap Activated by a Piezo-Induced Bending-Torsion Coupled Beam," *Journal of the American Helicopter Society*, Vol. 44, (1), January 1999.
2. Wang, D., Bartley-Cho, J., Martin, C., and Hallam, B., "Development of High-Rate, Large Deflection, Hingeless Trailing Edge Control Surface for the Smart Wing Wind Tunnel Model," *Proceedings of the SPIE – The International Society for Optical Engineering*, Vol. 4332, June 2001.
3. Koratkar, N., and Chopra, I., "Wind Tunnel Testing of a Smart Rotor Model with Trailing-Edge Flaps," *Journal of the American Helicopter Society*, Vol. 47, (4), October 2002.
4. Vasilescu, R., and Dancila, S., "Modeling and Analysis of Active Flap Using Coiled Bender Piezoelectric Actuators," *Journal of Intelligent Material Systems and Structures*, Vol. 15, September/October 2004.
5. Shaner, M., and Chopra, I., "Design and Testing of a Piezostack Actuated Leading-Edge Flap," *Proceedings of the*

SPIE – The International Society for Optical Engineering, Vol. 3668, June 1999.

6. Bernhard, A., and Chopra, I., “Hover Test of a Mach-Scale Rotor Model with Active Blade Tips,” *Journal of the American Helicopter Society*, Vol. 47, (4), October 2002.

7. Prechtel, E., and Hall, S., “An X-Frame Actuator Servo-Flap Actuation System for Rotor Control,” *Proceedings of the SPIE – The International Society for Optical Engineering*, Vol. 3329, July 1998.

8. Hall, S., Tzianetopoulou, T., Straub, F., and Ngo, H., “Design and Testing of a Double X-Frame Piezoelectric Actuator,” *Proceedings of the SPIE – The International Society for Optical Engineering*, Vol. 3985, June 2000.

9. Straub, F., Ngo, H., Anand, V., and Domzalski, D., “Development of a Piezoelectric Actuator for Trailing Edge Flap Control of Full Scale Rotor Blades,” *Smart Materials and Structures*, Vol. 10, (1), February 2001.

10. Lee, T., and Chopra, I., “Design of a Bidirectional Piezoelectric Actuator for Blade Trailing-Edge Flap,” *Proceedings of the SPIE – The International Society for Optical Engineering*, Vol. 4327, August 2001.

11. Chen, P., and Chopra, I., “Induced Strain Actuation of Composite Beams and Rotor Blades with Embedded Piezoceramic Elements,” *Smart Materials and Structures*, Vol. 5, (1), February 1996.

12. Chen, P., and Chopra, I., “Wind Tunnel Test of a Smart Rotor with Individual Blade Twist Control,” *Proceedings of the SPIE – The International Society for Optical Engineering*, Vol. 3041, June 1997.

13. Rodgers, J., and Hagood, N., “Preliminary Mach-Scale Hover Testing of an Integral Twist-Actuated Rotor Blade,” *Proceedings of the SPIE – The International Society for Optical Engineering*, Vol. 3329, July 1998.

14. Cesnik, C., and Shin, S., “On the Modeling of Integrally Actuated Helicopter Blades,” *International Journal of Solids and Structures*, Vol. 38, (10-13), March 2001.

15. Prahlad, H., and Chopra, I., “Design of a Variable Twist Tiltrotor Blade Using Shape Memory Alloy (SMA) Actuators,” *Proceedings of the SPIE – The International Society for Optical Engineering*, Vol. 4327, August 2001.

16. Shin, S., Cesnik, C., and Hall, S., “Closed-Loop Control Test of the NASA/Army/MIT Active Twist Rotor for Vibration Reduction,” *Journal of the American Helicopter Society*, Vol. 50, (2), April 2005.

17. Shin, S., Cesnik, C., and Hall, S., “Design and Simulation of Integral Twist Control for Helicopter Vibration Reduction,” *International Journal of Control, Automation, and Systems*, Vol. 5, (1), February 2007.

18. Bauchau, O., and Craig, J., *Structural Analysis: With Applications to Aerospace Structures*, Springer, Dordrecht, 2009.

19. Theodorsen, T., “General Theory of Aerodynamic Instability and the Mechanism of Flutter,” *NACA Report 496*, 1935.